Available online at www.sciencedirect.com

ScienceDirect

Mendeleev Commun., 2023, **33**, 306–310

Mendeleev Communications

New small-molecular benzimidazole derivatives for photovoltaics: synthesis, optical and electrochemical properties and application in perovskite solar cells

Sergei A. Kuklin,*[a,b] Sergey V. Safronov,[a] Oleg Yu. Fedorovskii,[a] Ekaterina A. Khakina,[a] Leonid V. Kulik,[c] Dmitry E. Utkin,[d] Lyubov A. Frolova,[b] Pavel A. Troshin[b] and Alexei R. Khokhlov[a]

[a] *A. N. Nesmeyanov Institute of Organoelement Compounds, Russian Academy of Sciences, 119334 Moscow, Russian Federation. E-mail: ineos-50@mail.ru*

[b] *Federal Research Center of Problems of Chemical Physics and Medicinal Chemistry, Russian Academy of Sciences, 142432 Chernogolovka, Moscow Region, Russian Federation*

[c] *V. V. Voevodsky Institute of Chemical Kinetics and Combustion, Siberian Branch of the Russian Academy of Sciences, 630090 Novosibirsk, Russian Federation*

[d] *A. V. Rzhanov Institute of Semiconductor Physics, Siberian Branch of the Russian Academy of Sciences, 630090 Novosibirsk, Russian Federation*

DOI: 10.1016/j.mencom.2023.04.003

New small molecule photovoltaic materials containing benzimidazole fragment were prepared by cross-coupling of the corresponding 1-bromo-4-(imidazol-2-yl)benzenes with multiborylated/stannylated polycyclic (het)arenes. Energies of HOMO/LUMO levels were calculated from cyclic voltammetry and UV/VIS spectroscopy data and are within the ranges –5.27...–5.73 and –2.33...–2.89 eV, respectively. Solar cells based on three different perovskites as light absorbing layers and compound SM7 as electron transporting material demonstrated power conversion efficiency values up to 10.78% without doping additives or perovskite engineering.

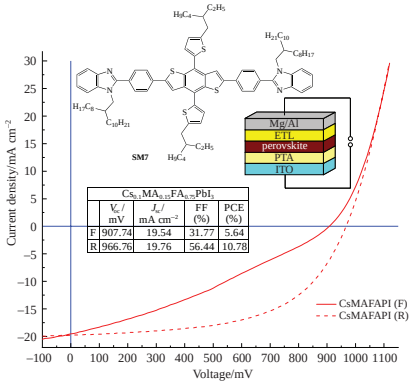

Keywords: benzimidazole derivatives, cross-coupling, small molecules, perovskite, solar cells, electron transfer materials, power conversion efficiency.

Currently, a large number of heterocyclic compounds has been recognized as promising materials for creating organic field effect transistors, light emitting diodes, photodetectors or solar cells.[1] An important requirement for such materials is high charge conductivity, which is increased by intermolecular π-stacking between aromatic molecules and the presence of intra- and intermolecular non-valent contacts, leading to formation of the most favorable molecular packing.[2,3] In turn, these two effects are enhanced by the introduction of heteroatoms into the structure of material molecules, which leads to the appearance of non-valent interactions,[2] *e.g.*, N···H, S···H, S···F. With this in mind, organic materials based on polyaromatic heterocyclic structures that possess the necessary properties for the design of organic electronic devices have been prepared.[4] Polyaromatic imidazole derivatives with semiconductor properties are of particular interest for organic electronics.[5] Imidazole derivatives can also serve as promising luminescent materials for organic light emitting diodes;[6,7] linear and branched imidazole chromophores of the donor–acceptor type have been synthesized. The chromophores exhibit nonlinear optical effects,[8] the magnitude of which strongly depends on the compound structure. 4,7-Bis{2-[(1-(2-ethylhexyl)-4,5-dicyanoimidazol-2-yl]vinyl}benzo[*c*][1,2,5]thiadiazole (EV-BT) with dicyanoimidazole fragments and its analogs were tested as acceptor materials in organic photovoltaics; however, the efficiency was only ~0.75%.[9–12] Later developed benzimidazole dyes for electrochemical Grätzel cells enabled to observe power conversion efficiency (PCE) of the order of 1.21–8.10%.[13–17]

The utilization of (benz)imidazoles as components of perovskite solar cells (PSCs) was more successful. The addition of imidazole and benzimidazole to the $PC_{60}BM$ electron transport layer of inverted PSCs enables to increase the efficiency up to 15.74–16.03%, mainly due to the improvement of the charge transport layer morphology.[18–20] Star-shaped compounds based on 1*H*-dithieno[3′,2′:3,4;2″,3″:5,6]benz[1,2-*d*]-imidazole were used as hole transport materials (HTMs) in conventional PSCs with the ITO/SnO_2/$FA_{0.85}MA_{0.15}PbBr_{0.45}I_{2.55}$/HTM/Au structure (MA and FA denote methylammonium and formamidinium cations, respectively); successful selection of peripheral substituents and the central fragment enabled to achieve the optimal morphology of the HTM layer and to reduce the number of defects, which led to high open-circuit voltage (V_{oc}), short-circuit current density (J_{sc}) and fill factor (FF) values. The maximum PCE was 16.90%, which is 0.55% higher than the values for 2,2′,7,7′-tetrakis[*N*,*N*-bis(4-methoxyphenyl)amino]-9,9′-spirobifluorene (spiro-OMeTAD), which was considered as one of the best hole transporting materials.[21] The use of 1,3-dimethyl-1*H*-thieno[3,4-*d*]imidazolium iodide derivative

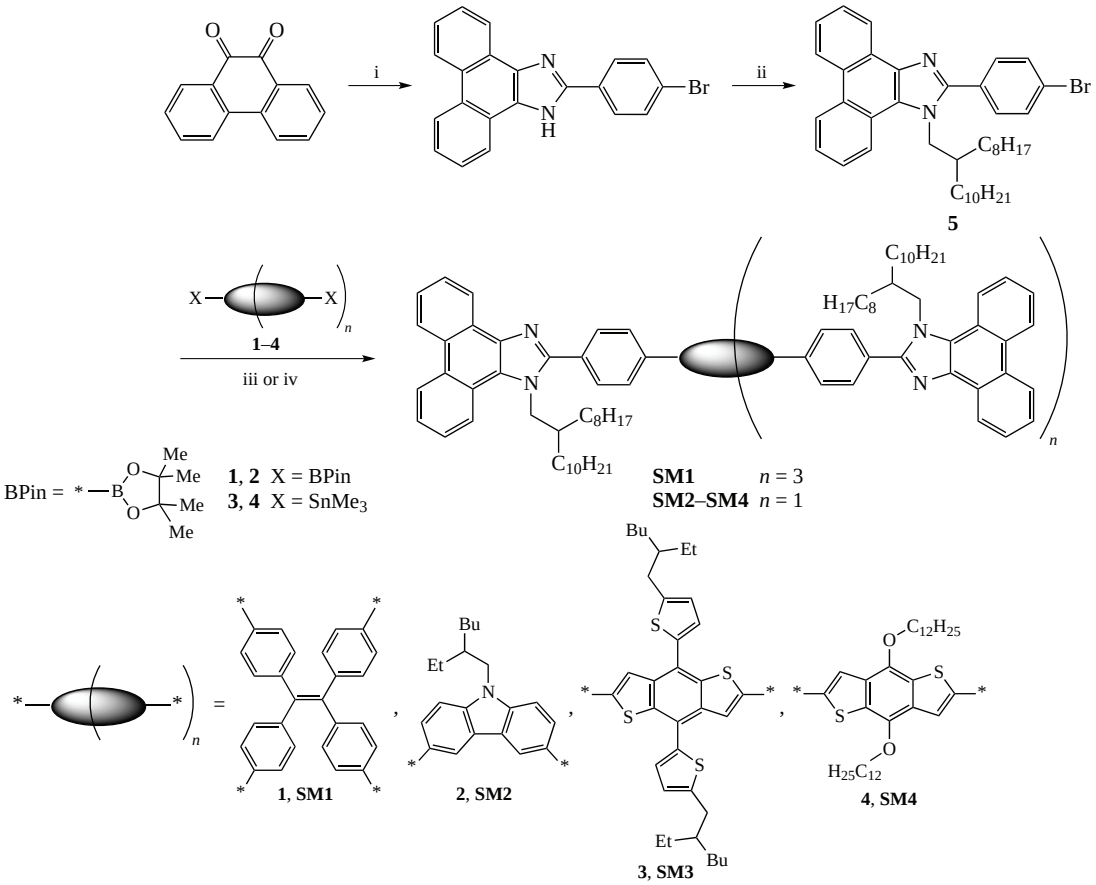

Scheme 1 *Reagents and conditions*: i, 4-BrC_6H_4CHO, $AcONH_4$, AcOH, 120 °C, 10 h; ii, $C_{10}H_{21}CH(C_8H_{17})CH_2Br$, K_2CO_3, DMF, 80 °C, 16 h; iii, $Pd(PPh_3)_4$, K_2CO_3, THF/H_2O, 80 °C, 48 h (for **1**, **2**), iv, $Pd(PPh_3)_4$, *o*-xylene, 150 °C, 16 h (for **3**, **4**).

(AI110) with three bis(4-methoxyphenyl)phenylamine substituents as an HTM provided an efficiency of 14.90% in p-i-n PSCs; it is of special note that this result was achieved without the use of doping additives.[22] The star-shaped derivative of 5-(7-methyl-2-(6′-methyl-[2,2′-bipyridin]-6-yl)-1*H*-benz[*d*]-imidazol-4-yl)thiophen-2-yl)ethane (YJS003), containing bis(4-methoxyphenyl)phenylamine and bipyridyl substituents, has favorable energies of frontier molecular orbitals with respect to the energy levels of perovskite $Cs_{0.05}FA_{0.78}MA_{0.17}PbI_{2.53}Br_{0.47}$ and good crystallinity, that reduces recombination losses at the interlayer boundary and enables to achieve PCE of 20.81%.[23]

Hybrid organic–inorganic solar cells based on light-absorbing perovskite layers feature the following advantages: high efficiency, low cost, and ease of manufacturing.[24] At present, the

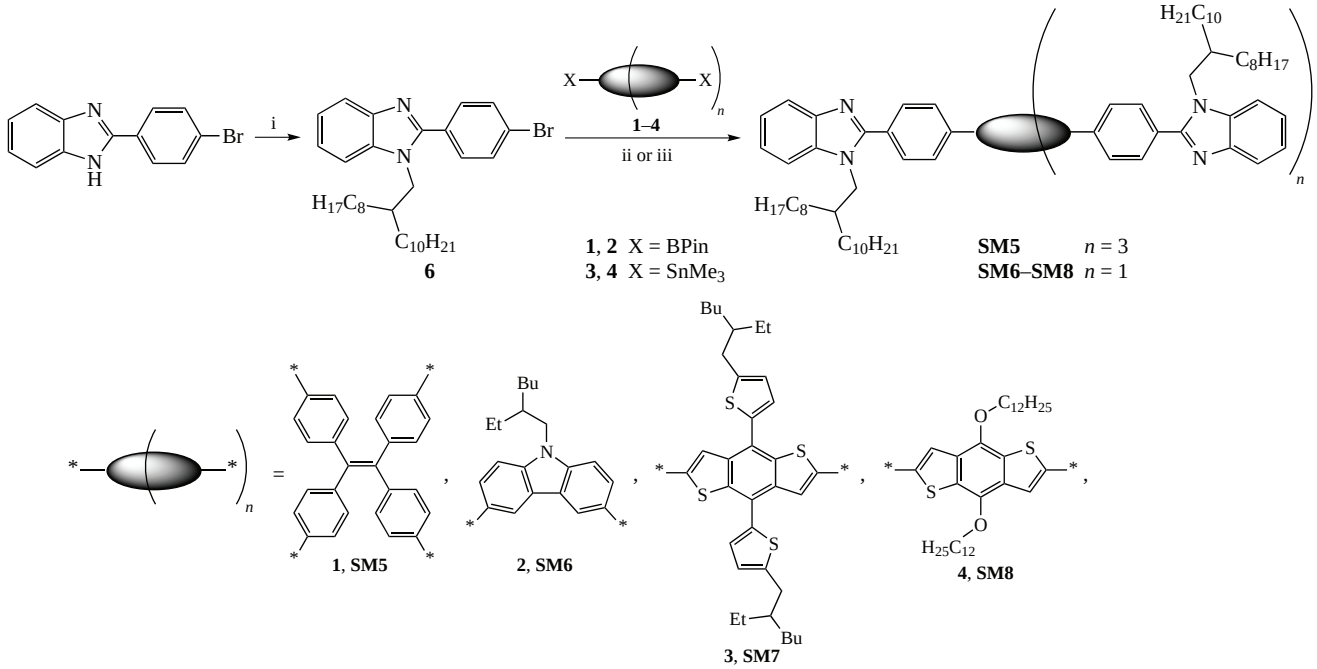

Scheme 2 *Reagents and conditions*: i, $C_{10}H_{21}CH(C_8H_{17})CH_2Br$, K_2CO_3, DMF, 80 °C, 16 h; ii, $Pd(PPh_3)_4$, K_2CO_3, THF/H_2O, 80 °C, 48 h (for **1**, **2**), iii, $Pd(PPh_3)_4$, *o*-xylene, 150 °C, 16 h (for **3**, **4**).

efficiency of PSCs has exceeded 25%, which practically corresponded to that of silicon-based photocells.[25] The main disadvantage of PSCs is their low stability associated with the low photostability of the organic materials used. Therefore, the search for new materials to create highly efficient PSCs with a long service life is relevant.[26,27] In view of results achieved using (benz)imidazole derivatives in perovskite photovoltaics, the study of their aryl-substituted derivatives and their quaternary salts looks promising. In this work, we synthesized a series of new low molecular compounds **SM1**–**SM8** with various central and terminal imidazole-containing groups and studied their optical and electrochemical properties. We also conducted a preliminary study of these compounds as components of PSCs based on various light-absorbing perovskite derivatives. For **SM7**-based solar cells, efficiencies of 6.24, 7.27, and 10.78% were observed using $MAPbI_3$, $Cs_{0.12}FA_{0.88}PbI_3$, and $Cs_{0.1}MA_{0.15}FA_{0.75}PbI_3$ perovskites, respectively.

New low molecular compounds **SM1**–**SM8** were obtained according to Schemes 1 and 2. The key step of the synthesis was the coupling between imidazole derivatives **5** and **6** equipped with bromobenzene moieties and organoelement cross-counterparts **1**–**4** bearing two or four reactive sites and appearing as central fragments in the final products **SM1**–**SM8**.

Benzimidazole derivative **5** (see Scheme 1) was obtained in a three-component reaction of 4-bromobenzaldehyde, ammonium acetate, and phenanthrene-9,10-dione. The subsequent alkylation with 2-octyldodecyl bromide afforded compound **5** in 61% yield. In turn, heterocyclization of *o*-phenylenediamine with 4-bromobenzoic acid followed by *N*-alkylation with 2-octyldodecyl bromide gave compound **6** (see Scheme 2, for details, see Online Supplementary Materials).

Absorption spectra of compounds **SM1**–**SM4** [Figure 1(*a*) and Table 1] have more pronounced bands in the short wavelength region (250–300 nm), apparently due to π–π* transitions within the phenanthrene fragments of the end groups, compared to **SM5**–**SM8**.

Compounds **SM3**, **SM4**, **SM7**, and **SM8** with benzodithiophene central fragments exhibit the longest wavelength absorption, and the absorption onset is about 470 nm in films. When tetraphenylethylene and carbazole are used as central blocks, the absorption edge is blue-shifted about 40 nm (**SM1**, **SM5**) and 60 nm (**SM2**, **SM6**), respectively. The values of the optical band gap (E_g^{opt}) are calculated by the formula $E_g^{opt} = 1240/\lambda_{onset}$, where λ_{onset} is the absorption edge of the film. The narrowest gap was observed for compounds **SM3**, **SM4**, **SM7** and **SM8** with benzodithiophene central fragments, for which the E_g^{opt} value is in the range of 2.62–2.66 eV. As for other compounds, the E_g^{opt} value varies in the range of 2.90–3.22 eV (see Table 1). The photoluminescence (PL) maxima in thin films are located approximately in the same region of 541–553 nm, except for **SM2** and **SM6** with carbazole fragments, for which the PL maxima are observed at 773 nm.

Cyclic voltammograms of **SM1**–**SM8** [Figure 1(*b*)] show one irreversible oxidation peak in the potential range (E_{ox}) of 0.471–0.926 V *vs*. ferrocene standard. The highest occupied orbital (HOMO) energies were calculated by the formula $E_{HOMO} = -e \times [E_{ox} + 4.80]$ (eV), and were in the range of –5.27...–5.73 eV. The energies of the lowest free orbitals (LUMO) were calculated by the formula $E_{LUMO} = E_g^{opt} + E_{HOMO}$ (eV) and varied in the range of –2.33...–2.89 eV. The energy level diagram for **SM1**–**SM8** [Figure 1(*c*)] shows that all compounds are rather wide-gap electron donors, so they may be used in organic and hybrid organic–inorganic electronic devices. The hole mobility (μ_h) values for the compounds were measured by SCLC method (see Table 1 and Figure S10) and the highest values 2.3×10^{-5} and 5.6×10^{-5} $cm^2\ V^{-1}\ s^{-1}$ were observed for **SM2** and **SM3**, respectively.

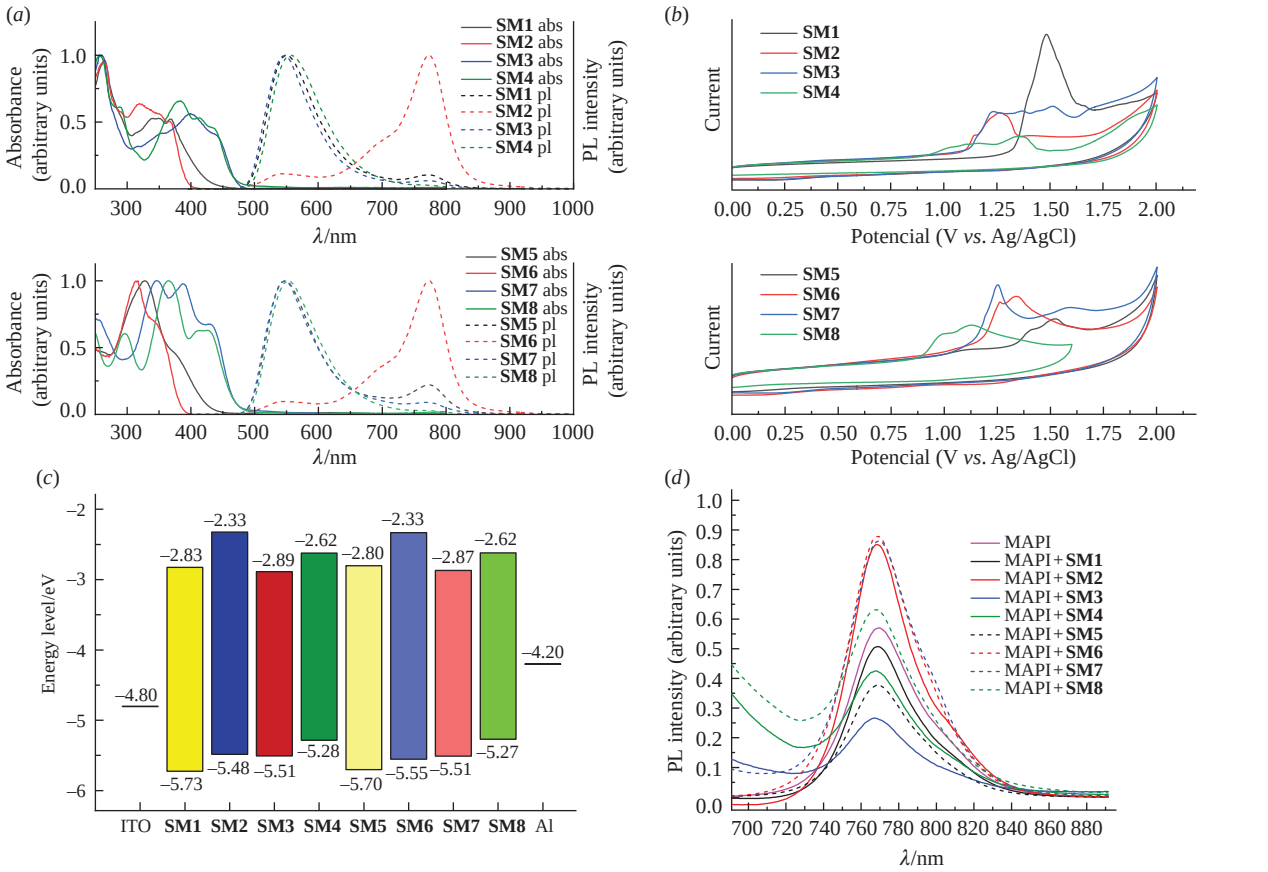

Figure 1 (*a*) Normalized absorption and photoluminescence spectra; (*b*) cyclic voltammograms; (*c*) energy levels diagram of films of **SM1**–**SM8** and (*d*) photoluminescence spectra of $MAPbI_3$ films coated with **SM1**–**SM8**.

Table 1 Absorption maxima, E_g^{opt} values, oxidation potentials, and HOMO/LUMO energies of compounds **SM1**–**SM8** in solid films.

SM	$\lambda_{abs\ max}$[a]/nm	λ_{onset}/nm	E_g[b]/eV	$\lambda_{em\ max}$[c]/nm	E_{ox}[d]/V	E_{HOMO}/eV	E_{LUMO}[e]/eV	μ_h[f]/cm^2 V^{-1} s^{-1}
SM1	265, 339, 350, 368	428	2.90	550, 774	0.926	–5.73	–2.83	9.7×10^{-6}
SM2	265, 320, 349, 368	393	3.16	541, 700, 773	0.685	–5.49	–2.33	2.3×10^{-5}
SM3	260, 353sh, 399, 438sh	473	2.62	547, 772	0.707	–5.51	–2.89	6.0×10^{-5}
SM4	257, 289, 383, 413, 435sh	466	2.66	558	0.484	–5.28	–2.62	3.8×10^{-6}
SM5	329, 368sh	427	2.90	547, 774	0.903	–5.70	–2.80	n.a.
SM6	315, 340sh	385	3.22	541, 700, 773	0.754	–5.55	–2.33	2.0×10^{-6}
SM7	250, 345, 388, 430	469	2.64	547, 768	0.710	–5.51	–2.87	5.6×10^{-6}
SM8	296, 363, 414, 424	468	2.65	553	0.471	–5.27	–2.62	n.a.

[a] Films were obtained from $CHCl_3$. [b] $E_g^{opt} = 1240/\lambda_{onset}$. [c] Measured under laser excitation at 445 nm. [d] Values *vs*. Fc, in 0.1 M Bu_4NPF_6 in MeCN, glass carbon working electrode, Pt counter electrode, Ag/AgCl reference electrode. [e] $E_{LUMO} = E_{HOMO} + E_g^{opt}$. [f] Measured by SCLC method for hole-only devices with ITO/PEDOT : PSS/**SM1**–**SM8**/Au structure.

Perovskite solar cells based on **SM1**–**SM8** were fabricated as follows. First, a thin layer of hole-transporting 'poly(bis(4-phenyl)(4′-methylphenyl)amine)' (PTA) was deposited on a thoroughly cleaned surface of a glass substrate with an electrically conductive layer of indium tin oxide (ITO) using a spin-coating process. After drying at 110 °C, a perovskite light-absorbing layer was applied on the PTA surface by a method involving the usage of an anti-solvent to obtain polycrystalline films. Next, an electron transport material (ETM), **SM1**–**SM8**, was deposited on the perovskite layer, over which electrode materials (Mg/Al or Al) were thermally deposited. Fullerene derivative $PC_{60}BM$ was used as a standard electronically conductive material. Initially, we studied p-i-n-architecture photocells with the ITO/PTA/$MAPbI_3$/ETL/Mg/Al structure, in which compounds **SM1**–**SM8** played the role of an electron transport layer (ETL). However, the obtained PCE values for most devices were not high and reached only 0.13...3.85%, mainly due to low values of J_{sc} and FF (for details, see Online Supplementary Materials). The maximum efficiency value of 6.24% (V_{oc} = 980 mV, J_{sc} = 18.21 mA cm^{-2}, FF = 34.94%) was observed for PSCs modified with **SM7** having the structural fragment 4,7-bis[5-(2-ethylhexyl)thiophene-2-yl]benzodithiophene and benzimidazole end groups.

We have conducted the PL study of $MAPbI_3$ films coated with **SM1**–**SM8** layers upon excitation at a wavelength of 445 nm. As it can be seen from Figure 1(*d*), upon deposition of **SM1**, **SM3**, **SM4**, and **SM5** films the perovskite PL intensity noticeably decreases. This indicated the extraction of charge carriers into the transport layer, whose efficiency grows in the rank **SM1** < **SM4** < **SM5** < **SM3**. In the case of **SM2**, **SM6**, **SM7**, and **SM8** films, the PL intensity of the perovskite increases, which may indicate partial passivation of structural defects on the surface of the perovskite film;[28,29] in the case of **SM8**, this effect is less pronounced. The maximum enhancement of perovskite luminescence is observed in the case of **SM2**, **SM6**, and **SM7** deposition. Obviously, this effect is associated with the structural features of these three compounds. Indeed, **SM2** and **SM6** have central carbazole fragments and end groups based on phenanthrenoimidazole and benzimidazole, respectively, and the enhancement of the PL signal does not depend on the type of the end group; in turn, **SM7** is based on 4,7-bis[5-(2-ethylhexyl)-thiophen-2-yl]benzodithiophene with end groups based on benzimidazole, and the transition to the phenanthrenoimidazole group (in **SM3**) causes quenching of perovskite luminescence. This suggests that the passivation of defects on the perovskite surface involves heteroatoms with lone electron pairs, which are located precisely in the central fragment of ETL molecules, but not in the end groups; terminal groups based on phenanthrenoimidazole rather prevent the manifestation of this effect, because being sterically bulkier, they can make it difficult for ETL molecules to approach surface defects, compared to benzimidazole-based end groups.

To improve the device efficiency, we investigated the most efficient compound (**SM7**) in PSCs based on two- and three-cation perovskites. When using dicationic perovskite $Cs_{0.12}FA_{0.88}PbI_3$ light absorbing layer in PSCs with the ITO/PTA/$Cs_{0.12}FA_{0.88}PbI_3$/**SM7**/Al structure, the best efficiency of 7.27% (V_{oc} = 888.97 mV, J_{sc} = 19.84 mA cm^{-2}, FF = 41.22%) was achieved, which is close to the performance of PSCs based on $MAPbI_3$. In the case of PSCs based on tricationic perovskite, ITO/PTA/$Cs_{0.1}MA_{0.15}FA_{0.75}PbI_3$/**SM7**/Al, a maximum efficiency of 10.78% was observed (V_{oc} = 967 mV, J_{sc} = 19.76 mA cm^{-2}, FF = 56.44%). The results of the study are presented in Figure 2 and Table 2.

According to Table 2, all PSCs studied are characterized by rather high voltages V_{oc} (0.75–0.98 V) and current densities J_{sc} (18.04–19.84 mA cm^{-2}). The maximum V_{oc} value of 0.978–0.980 V was observed for PSCs based on $MAPbI_3$, while the maximum J_{sc} values (19.68–19.84 mA cm^{-2}) were observed for devices based on $Cs_{0.12}FA_{0.88}PbI_3$. Devices based on $Cs_{0.12}FA_{0.88}PbI_3$ have a slightly lower external quantum efficiency (EQE) in the 600–800 nm wavelength range compared to devices based on the other two perovskites [see Figure 2(*b*)]. The values of the current densities obtained by integrating the EQE spectra of devices ($J_{sc,EQE}$) are in good agreement with the values obtained from the current–voltage characteristics (see Table 2). The main problem is the low values of the filling factors (FFs), which vary in the range of 25–56%, as well as a significant spread (hysteresis) of the values of V_{oc} and FFs during forward and reverse scanning of the applied voltage in the case of devices based on two- and three-cation perovskites [see Figure 2(*a*)]. This may indicate a non-optimal morphology of the charge-transport layer, the presence of a significant number of structural defects at interlayer boundaries, and, as a result, an imbalance in the transport of electrons and holes in photocells.[30]

In conclusion, eight new low molecular compounds **SM1**–**SM8** with central fragments based on tetraphenylethylene, *N*-alkylcarbazole, 4,8-bis[5-(2-ethylhexyl)thiophen-2-yl]benzo[1,2-*b*:4,5-*b*′]dithiophene and 4,8-didodecyloxybenzo[1,2-*b*:4,5-*b*′]dithiophene with end groups based on 1*H*-phenanthreno[9,10-*d*]imidazole and 1*H*-benzo[*d*]imidazole have been synthesized. Their properties have been systematically studied by absorption spectroscopy in the UV and visible regions, photoluminescent spectroscopy, and cyclic voltammetry. For PSCs based on **SM7**, power conversion efficiencies up to 10.78% were observed when using light-absorbing layers based on perovskites. This compound with terminal benzimidazole groups and a central benzodithiophene fragment is promising for electron transport layers in perovskite solar cells. Currently, we are aimed at improving the efficiency of photovoltaic cells based on it.

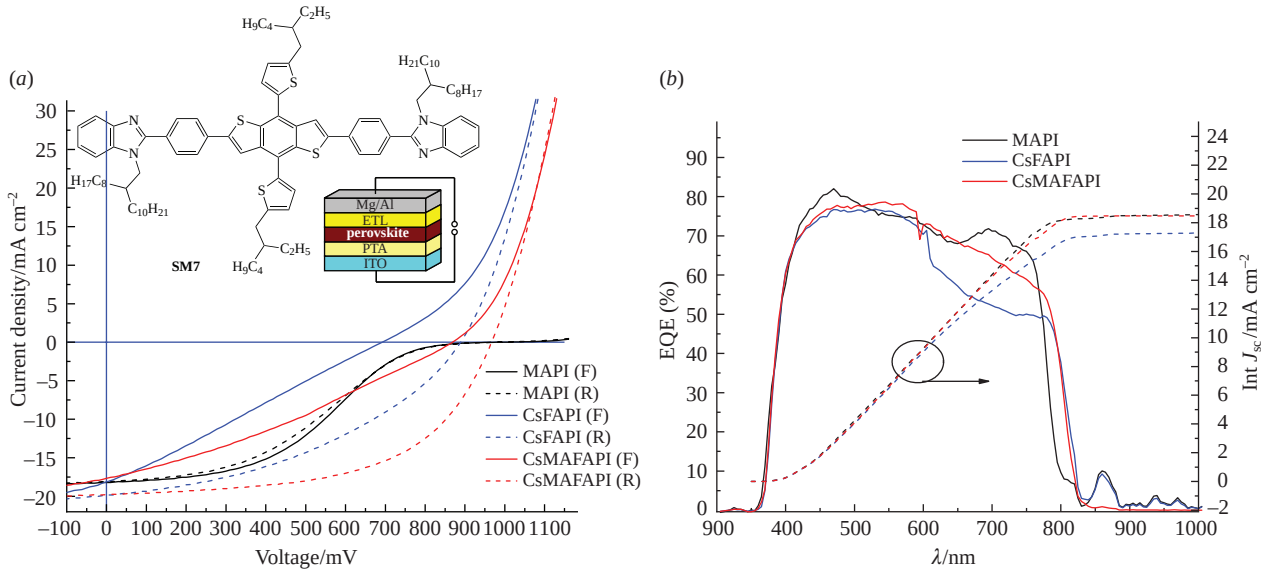

Figure 2 Some properties of PSCs ITO/PTA/$MAPbI_3$/**SM7**/Mg/Al, ITO/PTA/$Cs_{0.12}FA_{0.88}PbI_3$/**SM7**/Al and ITO/PTA/$Cs_{0.1}MA_{0.15}FA_{0.75}PbI_3$/**SM7**/Al: (*a*) current–voltage characteristics and (*b*) EQE spectra.

Table 2 Parameters of PSCs with ETL = **SM7** based on various perovskite layers.

Perovskite light absorbing layer[a]	Scan direction	V_{oc}/ mV	J_{sc}/ mA cm^{-2}	FF (%)	PCE (%)	$J_{sc\ EQE}$[b]/ mA cm^{-2}
$MAPbI_3$	F	980.45	18.21	34.94	6.24	18.53
	R	978.33	18.04	32.84	5.79	
$Cs_{0.12}FA_{0.88}PbI_3$	F	744.98	19.68	25.62	3.76	17.25
	R	888.97	19.84	41.22	7.27	
$Cs_{0.1}MA_{0.15}FA_{0.75}PbI_3$	F	907.74	19.54	31.77	5.64	18.46
	R	966.76	19.76	56.44	10.78	

[a] PSCs with the ITO/PTA/perovskite/**SM7**/Mg/Al structure were studied under illumination with a standard light source AM1.5 (100 mW), cell area was 0.08 cm^2. [b] Short circuit current density calculated by integrating the EQE spectrum.

This study was supported by the Russian Science Foundation (grant no. 22-23-00318). NMR, MALDI, UV-absorption and cyclic voltammetry studies and elemental analyses were performed with the financial support of the Ministry of Science and Higher Education of the Russian Federation employing the equipment of Center for molecular composition studies of INEOS RAS.

Online Supplementary Materials

Supplementary data associated with this article can be found in the online version at doi: 10.1016/j.mencom.2023.04.003.

References

1 *Organic Electronics Materials and Devices*, ed. S. Ogawa, Springer, Tokyo, 2015.
2 M. Klues and G. Witte, *CrystEngComm*, 2018, **20**, 63.
3 G. Han, Y. Yi and Z. Shuai, *Adv. Energy Mater.*, 2018, 1702743.
4 J. Li and Q. Zhang, *ACS Appl. Mater. Interfaces*, 2015, **7**, 28049.
5 M. Mamada, C. Pérez-Bolivar and P. Anzenbacher, Jr., *Org. Lett*., 2011, **13**, 4882.
6 S. Ye, S. Zhuang, B. Pan, R. Guo and L. Wang, *J. Inform. Display*, 2020, **21**, 173.
7 P. A. A. M. Vaz, J. Rocha, A. M. S. Silva and S. Guieu, *Materials*, 2021, **14**, 4298.
8 J. Kulhánek and F. Bureš, *Beilstein J. Org. Chem*., 2012, **8**, 25.
9 T. Kietzke, R. Y. C. Shin, D. A. M. Egbe, Z.-K. Chen and A. Sellinger, *Macromolecules*, 2007, **40**, 4424.
10 W. Zeng, K. S. L. Chong, H. Y. Low, E. L. Williams, T. L. Tam and A. Sellinger, *Thin Solid Films*, 2009, **517**, 6833.
11 Z. E. Ooi, T. L. Tam, R. Y. C. Shin, Z. K. Chen, T. Kietzke, A. Sellinger, M. Baumgarten, K. Mullen and J. C. deMello, *J. Mater. Chem*., 2008, **18**, 4619.
12 M. Schubert, C. Yin, M. Castellani, S. Bange, T. L. Tam, A. Sellinger, H. H. Hörhold, T. Kietzke and D. Neher, *J. Chem. Phys.*, 2009, **130**, 094703.
13 S. Sambathkumar, S. Priyadharshini, M. Fleisch, D. W. Bahnemann, G. Gnana Kumar, S. Senthilarasu and R. Renganathan, *Mater. Lett.*, 2019, **242**, 28.
14 M. Mao, X.-L. Zhang and G.-H. Wu, *Int. J. Photoenergy*, 2018, 2061472.
15 G. B. Bodedla, K. R. J. Thomas, M.-S. Fan and K.-C. Ho, *J. Org. Chem*., 2016, **81**, 640.
16 X. Chen, C. Jia, Z. Wan and X. Yao, *Dyes Pigm.*, 2014, **104**, 48.
17 J. Sivanadanam, I. S. Aidhen and K. Ramanujam, *New J. Chem*., 2020, **44**, 10207.
18 Y. Wang, Y. Yang, F. Uhlik, Z. Slanina, D. Han, Q. Yang, Q. Yuan, Y. Yang, D.-Y. Zhou and L. Feng, *Org. Electron.*, 2020, **78**, 105573.
19 Y. Wang, Y. Yang, D.-W. Han, Q.-F. Yang, Q. Yuan, H.-Y. Li, Y. Yang, D.-Y. Zhou and L. Feng, *Sol. Energy Mater. Sol. Cells*, 2020, **212**, 110553.
20 I. B. A. Ghani, M. Khalid, M. I. Hussain, M. M. Hussain, R. Ashraf and J. Wang, *Mater. Sci. Semicond. Process.*, 2022, **148**, 106788.
21 Q. Zeng, Y. Li, H. Tang, Y. Fu, C. Liao, L. Wang, G. Xing and D. Cao, *Dyes Pigm.*, 2020, **188**, 109241.
22 S. B. Akula, C. Su, Y.-T. Wang, Y. S. Tingare, B.-R. Chen, Y.-C. Jheng, Y.-J. Lin, H.-C. Lan, Y.-C. Chang, W. Lekphet and W.-R. Li, *J. Power Sources*, 2021, **483**, 229177.
23 Y. S. Tingare, C. Su, J.-H. Lin, Y.-C. Hsieh, H.-J. Lin, Y.-C. Hsu, M.-C. Li, G.-L. Chen, K.-W. Tseng, Y.-H. Yang, L. Wang, H. Tsai, W. Nie and W.-R. Li, *Adv. Funct. Mater.*, 2022, 2201933.
24 Z. Song, C. L. McElvany, A. B. Phillips, I. Celik, P. W. Krantz, S. C. Watthage, G. K. Liyanage, D. Apulb and M. J. Heben, *Energy Environ. Sci.*, 2017, **10**, 1297.
25 G. Ren, W. Han, Y. Deng, W. Wu, Z. Li, J. Guo, H. Bao, C. Liu and W. Guo, *J. Mater. Chem. A*, 2021, **9**, 4589.
26 L. Meng, J. You and Y. Yang, *Nat. Commun*., 2018, **9**, 5265.
27 M. F. Vildanova, A. B. Nikolskaia, S. S. Kozlov, O. I. Shevaleevskiy, O. V. Almjasheva and V. V. Gusarov, *Dokl. Phys. Chem.*, 2021, **496**, 13 (*Dokl. Ross. Akad. Nauk, Khim., Nauki Mater*., 2021, **496**, 63).
28 N. K. Noel, A. Abate, S. D. Stranks, E. S. Parrott, V. M. Burlakov, A. Goriely and H. J. Snaith, *ACS Nano*, 2014, **8**, 9815.
29 N. Ishida, A. Wakamiya and A. Saeki, *ACS Photonics*, 2016, **3**, 1678.
30 B. Chen, M. Yang, S. Priya and K. Zhu, *J. Phys. Chem. Lett*., 2016, **7**, 905.

Received: 18th November 2022; Com. 22/7046